




X-Ray absorption spectroscopy on airborne aerosols

Cite this: *Environ. Sci.: Atmos.*, 2022, 2, 1338

Muhammad H. Rashid, Camelia N. Borca, Jacinta M. Xto and Thomas Huthwelker *

Here we demonstrate a method for performing X-ray absorption spectroscopy (XAS) on airborne aerosols. XAS provides unique insight into elemental composition, chemical and phase state, local coordination and electronic structure of both crystalline and amorphous matter. The aerosol is generated from different salt solutions using a commercial atomizer and dried using a diffusion drier. Embedded in a carrier gas, the aerosol is guided into the experimental chamber for XAS analysis. Typical particle sizes range from some 10 to a few 100 nm. Inside the chamber the aerosol bearing gas is then confined into a region of about 1–2 cm³ in size, by a pure flow of helium, generating a stable free-flowing stream of aerosol. It is hit by a monochromatic X-ray beam, and the emitted fluorescent light is used for spectroscopic analysis. Using an aerosol generated from CaCl₂, KCl and (NH₄)₂SO₄ salt solutions, we demonstrate the functionality of the system in studying environmentally relevant systems. In addition, we show that the detection limits are sufficient to also observe subtle spectroscopic signatures in XAS spectra with integration times of about 1–2 hours using a bright undulator beamline. This novel setup opens new research opportunities for studying the nucleation of new phases in multicomponent aerosol systems *in situ*, and for investigating (photo-) chemical reactions on airborne matter, as relevant to both atmospheric science and also for general chemical application.

Received 7th March 2022
Accepted 26th September 2022

DOI: 10.1039/d2ea00016d

rsc.li/esatmospheres

Environmental significance

Atmospheric aerosols are complex mixtures of organics, electrolyte solutions or solid inorganic salts. They serve as catalysts in the atmosphere, contribute to photochemical processes, and are nuclei for cloud formation. Model experiments are key in deciphering the environmental functionality of aerosols. Experiments with airborne aerosols mimic natural environmental processes better than those using bulk matter. They are also advantageous because there is no sample-container contact, which could induce undesired chemical reactions or heterogeneous nucleation on sample container walls. However, spectroscopy on airborne matter is a significant analytical challenge, because the total amounts of material is very small. Here, we demonstrate that X-ray absorption spectroscopy, which can record electronic structure, oxidation state, local coordination and phase state, can be used for spectroscopic analysis of airborne matter. The presented new method paves an avenue to novel model studies for atmospherically relevant (photo-) chemical processes on aerosols, their formation, or for the nucleation of new phases, and hence their environmental impact.

Introduction

A myriad of chemical and physical process in the atmosphere involve micrometer-sized airborne particles, such as the destruction of stratospheric ozone, which is catalyzed by icy particles.^{1,2} Micrometer-sized particles also serve as nucleation sites for the formation of droplets and ice in clouds,^{3–5} and hence are key to the Earth's radiation balance⁶ and climate change. In addition, mixed organic aerosols also participate in tropospheric radical chemistry affecting levels of reactive oxygen species, and hence influencing human health.⁷ The main inorganic constituents of atmospheric aerosols are elements which are lighter than iron (*i.e.* O–Fe), including halogens, such as chlorine and bromine, or mixed organic sea-salt aerosols, with a significant aqueous fraction of sodium,

chlorine and sulfate.^{8,9} These elements can be found as ions in aqueous solutions, as precipitated crystallites, or embedded in organic matter. The chemical and physical state of these materials in a specific system then defines their chemical and physical function in the atmosphere.

Due to the microscopic size of aerosols particles, their chemical behavior differs from bulk material, which can affect the radical chemistry¹⁰ and photochemistry in aerosol droplets and particles.¹¹ In addition, microscopic airborne droplets can be useful in studying supersaturated matter. In a multicomponent aerosol droplet, nucleation occurs either by homogeneous or heterogeneous nucleation. The latter is seeded by contact of supersaturated matter with another interface, such as gas–liquid, liquid–solid, or other liquid phases or minerals, as it has been discussed for the nucleation of ice from aqueous solutions.¹² Nucleation studies are often hampered by unwanted heterogeneous nucleation on the walls of the sample container which can induce the nucleation of a new phase. This problem can be overcome by performing

Paul Scherrer Institute, Swiss Light Source, Laboratory for Femtochemistry, Forschungsstrasse 111, Villigen PSI, Switzerland. E-mail: Thomas.Huthwelker@psi.ch



environment. Once a photon is absorbed, the atom is in an excited or an ionized state with an electron-hole in an inner shell orbital. Then, the atom will decay back into the ground state by electronic transition of an electron into the empty inner-shell electron-hole. For example, an electronic transition from the L to the innermost K shell, will give rise to the X-ray emission $K\alpha$ line. The electronic transition into the ground state can also lead to the emission of an Auger electron. Measuring the transmission of photons through matter is the most direct measurement of the absorption coefficient. It is proportional to both the number of fluorescent photons, and the generated photoelectrons. Therefore, XAS spectra can also be measured by recording the total electron yield (TEY), which is given by the intensity of all emitted electrons, or by the X-ray emission line as function of the excitation energy. The X-ray fluorescence can be measured in air, if the photon absorption in the gas phase is not too high: for example, the transmission through 10 cm of air at 2 keV is less than 1%, but it is 99% through 10 cm helium. Hence, in the soft and tender X-ray range, it is advantageous to place the sample either in vacuum or in helium, as we do in the setup presented below. The total electron yield is mostly measured in vacuum, by simple detection of the electrical current into the sample, which measures the loss of electrons. This detection mode can also be implemented in an helium atmosphere, if the charge transport through the gas phase is well controlled.⁶³ A related detection method is X-ray photo electron spectroscopy (XPS), which analyzes the kinetic energy of the emitted photoelectrons. XPS

provides a direct picture of the electronic and chemical structure of elements in the surface region with a surface sensitivity in the sub nm range for soft X-rays. Total electron yield records all electrons including Auger electrons and therefore probes a somewhat thicker surface layer in the order of 1–10 nm for sub keV photons.^{64,65} In contrast, fluorescence detection probes bulk matter. Its probing depth is energy and material dependent. In the soft and tender X-ray range, the typical penetration depth in water ranges from a few 100 nm (at 200 eV) to 230 μm at 5 keV.

As analytical method, XAS is sensitive to very small amounts of material, in particular in the soft X-ray range. This can be directly concluded from the characteristic absorption length. Depending on the photon energies and materials, the probing depth in fluorescence mode ranges from the submicrometer range for soft X-ray up to some 100 μm for tender X-rays.

PHOENIX beamline

X-ray absorption spectroscopy measurements were performed at the PHOENIX (PHOTons for the Exploration of Nature by Imaging and XAFS) beamline at the Swiss Light Source (SLS, Villigen PSI), which covers both the soft and tender X-ray range (0.3 to 8 keV). This energy range is rarely served: there are only two main instruments in Europe: the LUCIA beamline (0.5–8 keV) at the Synchrotron Soleil⁶⁶ and the PHOENIX beamline⁶⁷ (0.3–8 keV) at the Swiss Light Source (SLS). An elliptical undulator serves as photon source for linear and elliptically polarized photons. There are two branchlines:



Fig. 1 Experimental setup for the generation of aerosols. (a) Aerosols are generated using a commercial nebulizer, which is operated using compressed nitrogen. (b) Schematic of the flow system for aerosol generation and coupling to the endstation. HPLC: high performance liquid chromatography pump, DC: droplet collector to prevent contamination of mass flow controllers, V1: 3-way valve to add reactive gases, V2: option to add additional N_2 to reduce humidity, V3/V4: valves to switch dryer on/off, V5: regulation valve to regulate pressure in endstation, V6: needle valve for additional N_2 flow to reduce humidity in vacuum pump, P: vacuum gauge, RH: humidity sensor, FC1: gas flow controller for nebulizer, FC2: gas flow controller to change humidity level, FC3: gas flow controller for backflow into chamber. An additional aerosol filter (not shown) protects the vacuum pump from contamination with particles.



pumped out of the endstation *via* outlet B together with all gases entering the endstation. Using this arrangement, the particle free He backflow confines the airborne particle stream into a small volume between inlet A and outlet B, preventing any contamination of the experimental endstation with aerosol particles.

The functionality of the system is demonstrated in Fig. 2b, which shows a photo of the set up mounted in the experimental chamber of the beamline. The trapezoid shows the region where the aerosol flow is confined between inlet A and outlet B. Here, a laser diode illuminates a part of the region between the in- and outlets where the aerosol reflects the laser beam. This demonstrates that the aerosol flow is nicely confined to the region between inlet and outlet.

Pressure regulation

For a reliable operation of the setup, both gas flows and pressure in the chamber must be kept very stable, and were therefore controlled by mass flow controllers (manufacturer: Bronkhorst). The pressure in the endstation was regulated by computer controlled needle valve (manufacturer: Pfeiffer, type RME-005A) at the exit of outlet B to keep the chamber pressure constant. To protect this valve from clogging with aerosols, a metal tube (38 mm inner diameter, 15 cm length) filled with household cotton wool, was placed before the regulation valve. Using this method, the pressure in the chamber can be stabilized within 0.1% in the range of 600–800 mbar.

SiN window

The beamline, operating in high vacuum ($<10^{-7}$ mbar), is separated from the endstation by a silicon nitride window (0.5 μm thick), which serves as main gas barrier. To protect this window, a second safety barrier, namely a Kapton foil (7 micron thickness, about 80% transmission at 3 keV) was mounted directly over the window. In case the silicon nitride window breaks, the Kapton foil would be pressed onto the frame of the silicon nitride window by the gas in the endstation. This would slow down the

venting of a small chamber between beamline optics and endstation, leaving time to close the additional automated shutter to the beamline, and providing additional safety to protect the beamline from contamination with aerosols.

SDD detector

The emitted fluorescence from the aerosols was measured using a silicon drift detector (SDD, manufacturer Ketek, Germany). The detector is mounted in a 90 degree angle relative to the incoming beam. The sensitive detector window was protected using an additional Kapton foil (7 μm thickness). Furthermore, a protective cone ensured that particles could not contaminate the Kapton foil, and that only fluorescent light originating from the aerosol stream can reach the detector, excluding X-ray fluorescence from the stray contamination in the chamber. The SDD detector was operated using the Falcon readout electronics (manufacturer: XIA LCC, Oakland, USA) in an energy dispersive mode.

Feasibility considerations

The spectroscopy of airborne aerosols using XAS is challenging due to the very small amount of airborne condensed matter. For example, an assumption of 3×10^6 airborne particles with a radius of 0.1 μm , corresponds to an effective thickness of the solid phase of about 0.13 nm per 1 cm of pathlength. To assess the feasibility of measurements on such a thin film of an aqueous solution in transmission geometry, we first note that the X-ray absorption in water for energies below 1 keV is mostly larger than 5%, but decreases for the higher tender X-rays. Hence, the overall optical density of the aerosol is small, but could be sufficient for transmission spectroscopy at the O-K edge. However, the total absorption of a 1 M CaCl_2 solution is about 0.4% at the Cl K edge (2822.4 eV), and about 0.2% at the Ca-K edge (4038.5 eV), with an expected XAS edge step in the order of 0.1–0.3%. Since this is too low for transmission spectroscopy and we aim for bulk spectroscopy, here we measure XAS spectra in fluorescence mode.

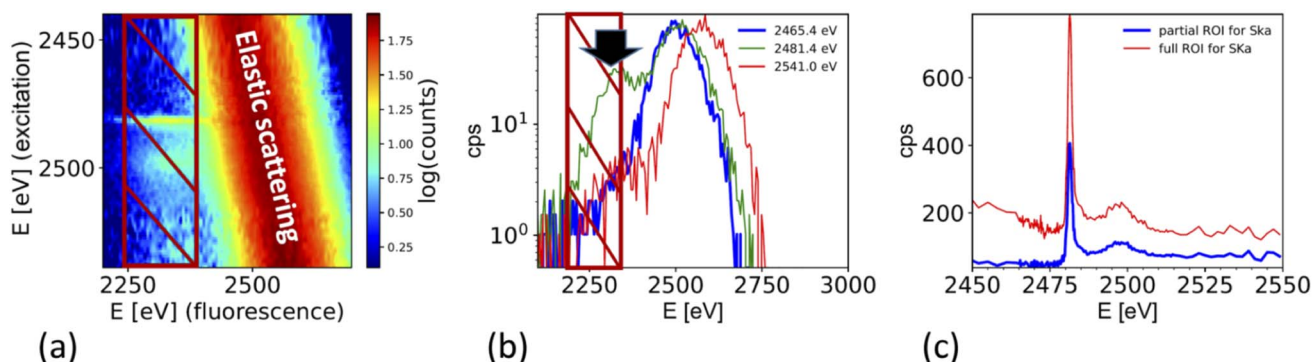


Fig. 3 (a) X-ray fluorescence line $\text{S K}\alpha$ (hatched region) and elastic scattering line for different excitation energies. (b) Cross section through (a) for different excitation energies illustrates the interference of the elastic scattering with the $\text{S K}\alpha$ fluorescence. Black arrow marks the exact location of the $\text{S K}\alpha$ emission line at 2308 eV. (c) Derived XAS spectrum from $\text{S K}\alpha$ emission line for two cases. Case 1 'full ROI' integrates over the full width of the emission line (as indicated in (a)), while the case 'partial ROI' integrates over the range avoiding the background by the elastic scattering as indicated in (b). The figure shows the raw data without normalization by I_0 . Note that (b) shows one single S XAS scan, while the data in Fig. 5 is an average of 4 single scans.



edge XANES spectra for drying ammonium sulfate, can be in between the ones for an aqueous solution and fully crystallized matter.

Summarizing, the spectrum taken from the aerosols is consistent with the one from the solid references. The spectra show that the drying of the aerosol particles indeed caused the rapid crystallization of ammonium sulfate from the airborne microdroplets. We note that the strong presence of elastic scattering hampers the normalization of the spectra, which may be one reason why the intensity of the white line at 2481.3 eV seems higher for spectra taken from aerosols compared to the one taken from the references. In general, line intensities in XAS can be affected by normalization artifacts or over-absorption, in contrast to peak positions and spectral features. We have tried different normalization parameters, leading to different results for the white line intensity, but keeping all structural features the same.

Calcium chloride containing aerosol

Ca K-edge spectra. Fig. 6 compares XAS spectra taken from 3 different aqueous CaCl_2 solutions (0.1 M, 0.5 M and 2.5 M), with a reference spectrum taken from solid CaCl_2 (dashed line in Fig. 6a in TEY), and a dilute bulk solution (10 mM CaCl_2). Clearly, the aerosol spectra resemble the solution spectrum, and not the one of a solid. The main white line position is shifted towards lower energies when compared with the spectra of a dilute solution (marked as A in Fig. 6a).

Furthermore, the edge of the aerosol spectra (see arrow marked as B in Fig. 6a) shows a shoulder, which is less marked in the spectra of a dilute solution. This observation is consistent with the work by Fulton and co-workers,^{73,74} who compared

a diluted solution with Ca^{2+} ions with a 6 M solution of CaCl_2 . In this work also the white line peak shifted towards lower energies and a shoulder feature (around 4045 eV) is unfolded in the concentrated solution (2.5 M spectrum in Fig. 6a).

These spectral features contain important structural information about the coordination of the Ca^{2+} ions, and hence are relevant for the ion's chemical role. The spectra can be interpreted following Fulton and co-workers:⁷⁴ the main peak at 4050/4049 eV is primarily due to the single scattering along the Ca–O pathway, and is characteristic for the presence of a fully hydrated Ca^{2+} ion. The 1s to 4p transition (feature B) and the slight shift of the white line is also visible in the solid $\text{CaCl}_2 \cdot 6\text{H}_2\text{O}$ structure (not shown, see ref. 74). Hence, the similarity of the spectra from the aerosol sample with the one of $\text{CaCl}_2 \cdot 6\text{H}_2\text{O}$ indicates that the aerosol samples have a fully hydrated Ca^{2+} ion, and that the Cl^- is present only in the second coordination shell. Therefore, the spectra from the aerosol droplets resemble the spectra of a highly concentrated CaCl_2 solution (several M concentration). We note that the white line appears to be the highest for spectra taken from the highest starting concentrations. However, this effect could be an artifact from the elastic scattering present in the spectra, as demonstrated in Fig. 3 and in the discussion of the ammonium sulfate spectra above. This contribution is hard to quantify and increases for low concentrations and hampers the normalization procedure for XAS spectra, such that relative peak ratios can be affected. However, peak positions and shape features, such as the observed shoulder of the peaks remain unaffected.

Cl K-edge spectra. Fig. 6b compares the spectra from a solid CaCl_2 reference (black dashed line), with the XAS spectra generated from nebulized dried solutions with 0.1 and 2.5 M solutions of CaCl_2 (blue and red lines), and with a 0.5 M bulk

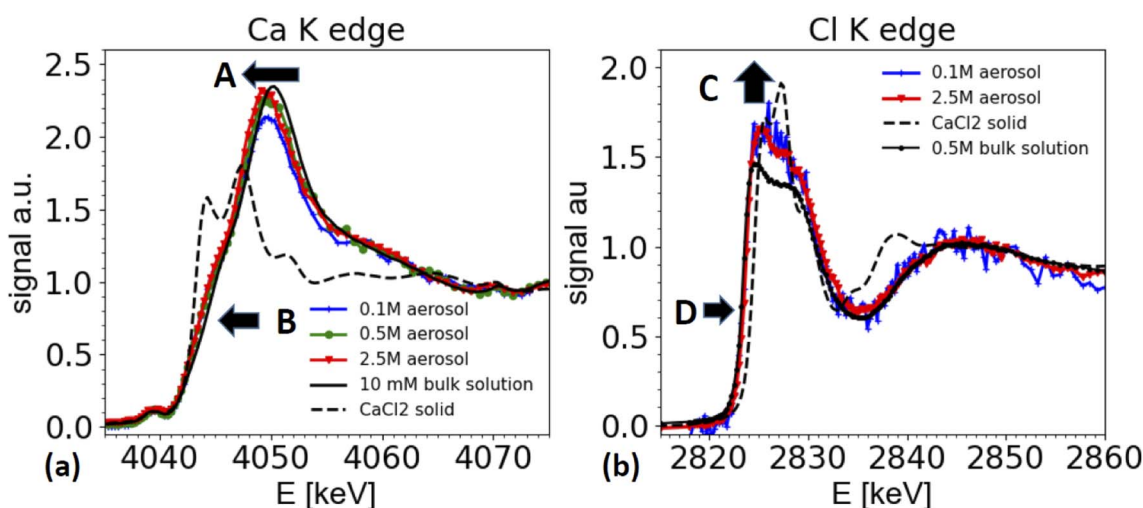


Fig. 6 XAS spectra from nebulized solutions with different CaCl_2 starting concentrations after passing the dryer and comparison with spectra taken from bulk solutions and solid references. (a) Ca K-edge spectra from airborne aerosols, generated from nebulized solutions of 0.1 M, 0.5 M and 2.5 M CaCl_2 (blue, green, red lines, respectively), compared with a spectrum from a 0.5 M CaCl_2 solution (black), and solid CaCl_2 (dashed black line) measured in TEY mode. Arrow A marks the shift of the white line energy of aerosol samples relative to the dilute bulk solution. Arrow B marks the enhanced shoulder region for aerosol samples. (b) Cl K edge spectra from airborne aerosols generated from a CaCl_2 solution of 0.1 M, and 2.5 M solutions (blue and red lines, respectively) compared with a XAS spectrum taken from a 0.5 M bulk solution (black line, corrected for over-absorption) and CaCl_2 solid (dashed line). Arrow D points towards a slight shift of the edge position of the aerosol sample compared to the solution of a dilute reference. The data for the Ca K-edge spectra were smoothed using a boxcar smoothing of 2 bin width.



solution of CaCl_2 (black line). Similar to the Ca K-edge, the absorption spectra taken from aerosols are not consistent with the one of a CaCl_2 solid reference (dashed line in Fig. 6b), but resemble the reference spectra taken from a 0.5 M CaCl_2 solution. The XAS spectra are also very similar to the spectra of HCl solutions,⁷⁵ where the $\text{Cl}^-/\text{H}_3\text{O}^+$ ion pair is dominant.

Two differences can be observed in Fig. 6b. First the intensity of the 'white line' region line (2824–2828 eV) is slightly enhanced for the aerosol spectra compared to the one of the reference solution (marked as C in Fig. 6b). In XAS, white line intensities always need to be taken with some care, as they can be hampered by over-absorption, but also by normalization artifacts. Other than for the ammonium sulfate spectra shown in Fig. 5, here the white line intensity was insensitive to changes of normalization parameters, and hence is more reliable, but still needs to be taken with care, as it could be affected by systematic errors in the over-absorption correction for the spectrum from the 0.5 M bulk solution. Secondly, and more importantly, there is a slight shift of the edge position of the white line by about 0.3 eV towards higher energies for the spectra taken on aerosols compared to the ones of the bulk solutions (marked as D in Fig. 6b).

We note that a similar shift of the white line has also been observed by Fulton and co-worker,⁷⁵ when comparing a 2.5 M NaCl solutions with various HCl solutions of much higher concentration. While the solutions of HCl and CaCl_2 contain different cations, they have the same anion, namely Cl^- . As XAS is local probe, the Cl K edge XANES spectra probe the local coordination around the Cl^- ion, and hence similar trends can be expected in both solutions.

Due to the water loss during dehydration of the droplets, the CaCl_2 concentration in the droplets increases and the droplet concentration adjusts to the humidity at the exit of the dryer. In this specific experiment, we are not certain whether we really reached a relative humidity below the deliquescence humidity (32% rh) of CaCl_2 , as the humidity at the dryer's exit was not measured, and the formation of liquid water was observed in the entry region of the dryer. Hence, we cannot be certain

whether the solution in the droplets is indeed supersaturated. However, the signature of the XAS spectra are clearly consistent with a very concentrated solution.

Nebulized KCl solution and CaCl_2/KCl mixed solution

To demonstrate the feasibility of studying mixed systems, an aerosol was generated from a pure KCl solution (0.2 M) and from mixed KCl/CaCl_2 solutions of different K/Ca molar ratio ranging from 5 : 1 (0.5 M of KCl) to 1 : 10 (0.05 M of KCl). The results are summarized in Fig. 7 and compared with a XAS spectrum taken from crystalline KCl. For aerosols generated from a pure KCl solution and from the 5 : 1 and 1 : 5 solutions, the XAS spectrum are consistent with the one of crystalline KCl. Hence the particles quickly crystallize within 1–2 seconds after passing the dryer. The timescale is estimated from the gas flow rate, tube length and diameter. This observation is consistent with the known deliquescence humidity for KCl of 85%,⁷⁶ which is well above the humidity at the dryer's exit.

Interestingly, the spectrum of an aerosol nebulized from a solution with a 1 : 10 KCl/CaCl_2 ratio does not show the characteristic peaks of crystalline KCl, as illustrated in Fig. 7b. The spectrum appears featureless, as typical for the spectra of ions in amorphous or aqueous environments. However, the main peak is around 3614 eV, about 3 eV below the maximum intensity found in the reference spectra from a 0.5 M KCl solution, making the spectrum also inconsistent with the one of a 0.5 M KCl solution. A detailed analysis of this spectrum is beyond the scope of this paper. We note that Deng and coworkers,⁷⁷ studied the formation of CaCl_2 and KCl in concentrated mixed solution, and reported the presence of crystalline KCl for a K/Ca ratio of 0.1, but not for K/Ca of 0.07 and lower, which indicate that KCl either does not form in the presence of concentrated CaCl_2 , or that its formation is kinetically hindered. This example shows that it is possible to spectroscopically analyze the chemical structure of mixed systems in airborne particles, where the smaller component is in the order of 10% of the total material.



Fig. 7 Comparison of K-K edge XAS spectra taken from aerosol generated from various KCl/CaCl_2 aqueous solutions compared with references. (a) XAS spectra from aerosols generated from a pure 0.2 M aqueous KCl solution (blue dots) and solutions with different K/Ca ratio; green dots: K/Ca = 5 : 1, with 0.5 M KCl; magenta K/Ca = 1 : 5 KCl with 0.1 M KCl, compared with a spectrum of crystalline KCl (black line) measured in TEY mode. (b) XAS spectrum taken from a 1 : 10 K/Ca solution with 0.05 M KCl (blue), compared with a spectrum from crystalline KCl, and of a 0.5 M KCl solution (corrected for over-absorption). Chamber pressure was 600 mbar, except for the 1 : 10 K/Ca solution, where the pressure was 500 mbar. Elemental ratios refer to molar ratios.



Conclusion

Proof of concept for aerosol spectroscopy

A new setup for performing X-ray absorption spectroscopy in the tender X-ray regime on a free-flowing stream of airborne aerosol particles is presented. As proof of concept, a simple system was employed involving the crystallization of inorganic salts from nebulized solution droplets. The sensitivity of the system was found to be sufficient for studying pure airborne particles. In addition, the findings show that it is feasible to measure XAS spectra from components in the aerosol particles, if they are in the order of 10% of the main aerosol content. Typical integration times for the spectra shown were in the order of 1–3 hours.

Complementarity to aerosol lens systems

The presented approach is complementary to systems which employ aerosol lenses to inject the aerosol as a thin jet into a low-pressure chamber, which may change the thermodynamic state of the matter during its flight through the aerosol lens. For operation of an aerosol lens system, in particular when connected to XPS⁵¹ low pressures are needed. For XAS at tender X-rays, this boundary condition can be relaxed as the photon absorption in the gas phase is sufficiently low if helium is used. The presented experiments were performed at the same pressure in the aerosol flow system from sample preparation, during chemical processing in the flow system, all the way down to the point of spectroscopic analysis. Hence, the thermodynamic state of the aerosol particles can be controlled during the whole process from sample generation to spectroscopic analysis.

Potential future applications in atmospheric sciences

The presented experimental approach aims to perform model laboratory experiments to decipher fundamental chemical processes in airborne aerosols. As XAS probes the local coordination of atoms in matter, the physical and chemical phase state and electronic properties, one can envision a wide range of applications in many scientific fields. For example, the technique could address important questions related to the chemistry of atmospheric aerosols, such as the study of the oxidation state of aerosol constituents in redox systems. Another important application is the *in situ* study of the phase state of non IR active inorganic matter in mixed organic aerosols. Here, *in situ* XAS experiments could directly probe the chemical state of the inorganic fraction in the aerosols. Moreover, photochemistry could be another important potential research field, where XAS could be applied to study photochemical processes in aerosols. With a residence time of individual droplet in the order of 1–2 ms in the measurement region, photochemical processes faster than 1 ms could be studied by direct illumination of the sample with light, using pump probe data acquisition schemes. For the study of slower systems, a photochemical reactor with longer residence time could be added into the flow system to process the aerosol prior to measurement.

Nucleation studies

The described experiment opens a novel avenue to study supersaturated systems, or the nucleation of new phases. This question is obviously highly relevant to atmospheric sciences, but also to fundamental questions in synthetic chemistry. Nucleation studies can be seriously hampered by sample container interfaces, which may induce heterogeneous nucleation. Once nucleation occurs in a bulk sample, often rapid growth of the freshly nucleated new phase occurs, which makes it difficult to study the very first moments and products of the nucleation process. Such problems can be solved by using a constant stream of airborne particles or droplets, which serve as a large number of identical chemical ‘micro-reactors’. With all airborne droplets suffering equal chemical treatment, such as drying, the addition of gases which may induce crystallization, or cooling, one would generate statistically relevant averaged information about the system’s behavior. As the aerosols are small there would be practically no diffusive barriers inside of the aerosol droplets, and with gas flow speeds of more than 1 m s⁻¹ in tubes, and 1 m distance between the region where the crystallization is induced, typical timescales of 1 second or less can be studied, in an experiment operating with a steady state gas flow. With residence time of milliseconds for individual particles in the measurement region itself, also shorter timescales of some 10 ms can be envisioned, if the zone where nucleation is induced is brought close to the measurement zone. Currently, the experiment is operated at an ambient pressure of 500–700 mbar of helium, which would fundamentally allow to study even the oxygen K edge (543.1 eV). Hence, it would be conceivable to further develop the setup and to study the effect of impurities on ice nucleation. While atmospheric science is one of the key applications for this instrumentation, applications in other fields are conceivable, in particulate in liquid phase, nanoparticle and synthetic chemistry.

Author contributions

TH: conceptualization, investigation, formal analysis, methodology, funding acquisition, supervision, writing-original draft, instrument development; CB: investigation, writing-review & edit, formal analysis, visualization; JMX: investigation, writing-review & edit, instrument development; MHR: investigation, writing-review & edit, formal analysis, instrument development.

Conflicts of interest

There are no conflicts of interest to declare.

Acknowledgements

We gratefully acknowledge the fantastic technical support from Reto Wetter and Christophe Frieß for all experimental setups. We thank Dr J. N. Fulton for providing raw data from previous experiments for comparison. We thank Dr M. Ammann for helpful discussions around the aerosol generation and setup and for providing a dryer for aerosols. The authors would like to thank the Swiss National Science Foundation (SNSF) for



- J. P. D. Abbatt, J. Y. Aller, A. K. Bertram, D. A. Knopf and B. J. Murray, A marine biogenic source of atmospheric ice-nucleating particles, *Nature*, 2015, **525**, 234–238.
- 29 J. F. Creemer, S. Helveg, G. H. Hoveling, S. Ullmann, A. M. Molenbroek, P. M. Sarro and H. W. Zandbergen, Atomic-scale electron microscopy at ambient pressure, *Ultramicroscopy*, 2008, **108**, 993–998.
- 30 E. de Smit, I. Swart, J. F. Creemer, G. H. Hoveling, M. K. Gilles, T. Tylizszczak, P. J. Kooyman, H. W. Zandbergen, C. Morin, B. M. Weckhuysen and F. M. F. de Groot, Nanoscale chemical imaging of a working catalyst by scanning transmission X-ray microscopy, *Nature*, 2008, **456**, 222–U239.
- 31 I. J. Drake, T. C. N. Liu, M. Gilles, T. Tylizszczak, A. L. D. Kilcoyne, D. K. Shuh, R. A. Mathies and A. T. Bell, An *in situ* cell for characterization of solids by soft x-ray absorption, *Rev. Sci. Instrum.*, 2004, **75**, 3242–3247.
- 32 T. Huthwelker, V. Zelenay, M. Birrer, A. Krepelova, J. Raabe, G. Tzvetkov, M. G. C. Vernooij and M. Ammann, An *in situ* cell to study phase transitions in individual aerosol particles on a substrate using scanning transmission X-ray microspectroscopy, *Rev. Sci. Instrum.*, 2010, **81**, 113706.
- 33 S. T. Kelly, P. Nigge, S. Prakash, A. Laskin, B. B. Wang, T. Tylizszczak, S. R. Leone and M. K. Gilles, An environmental sample chamber for reliable scanning transmission x-ray microscopy measurements under water vapor, *Rev. Sci. Instrum.*, 2013, **84**, 073708.
- 34 C. H. M. van Oversteeg, H. Q. Doan, F. M. F. de Groot and T. Cuk, In situ X-ray absorption spectroscopy of transition metal based water oxidation catalysts, *Chem. Soc. Rev.*, 2017, **46**, 102–125.
- 35 L. G. Wang, J. J. Wang and P. J. Zuo, Probing Battery Electrochemistry with In Operando Synchrotron X-Ray Imaging Techniques, *Small Methods*, 2018, **2**, 20.
- 36 V. Zelenay, M. Ammann, A. Krepelova, M. Birrer, G. Tzvetkov, M. G. C. Vernooij, J. Raabe and T. Huthwelker, Direct observation of water uptake and release in individual submicrometer sized ammonium sulfate and ammonium sulfate/adipic acid particles using X-ray microspectroscopy, *J. Aerosol Sci.*, 2011, **42**, 38–51.
- 37 V. Zelenay, M. E. Monge, B. D'Anna, C. George, S. A. Styler, T. Huthwelker and M. Ammann, Increased steady state uptake of ozone on soot due to UV/Vis radiation, *J. Geophys. Res. Atmos.*, 2011, **116**, DOI: [10.1029/2010JD015500](https://doi.org/10.1029/2010JD015500).
- 38 R. E. O'Brien, B. B. Wang, S. T. Kelly, N. Lundt, Y. You, A. K. Bertram, S. R. Leone, A. Laskin and M. K. Gilles, Liquid-Liquid Phase Separation in Aerosol Particles: Imaging at the Nanometer Scale, *Environ. Sci. Technol.*, 2015, **49**, 4995–5002.
- 39 R. I. Kaiser and A. G. Suits, A high-intensity, pulsed supersonic carbon source with C(P-3(j)) kinetic energies of 0.08–0.7 eV for crossed beam experiments, *Rev. Sci. Instrum.*, 1995, **66**, 5405–5411.
- 40 C. Nicolas, J. N. Shu, D. S. Peterka, M. Hochlaf, L. Poisson, S. R. Leone and M. Ahmed, Vacuum ultraviolet photoionization of C-3, *J. Am. Chem. Soc.*, 2006, **128**, 220–226.
- 41 M. Ahmed and O. Kostko, From atoms to aerosols: probing clusters and nanoparticles with synchrotron based mass spectrometry and X-ray spectroscopy, *Phys. Chem. Chem. Phys.*, 2020, **22**, 2713–2737.
- 42 C. Weeraratna, O. Kostko and M. Ahmed, An investigation of aqueous ammonium nitrate aerosols with soft X-ray spectroscopy, *Mol. Phys.*, 2022, **120**, e1983058.
- 43 M. I. Jacobs, B. Xu, O. Kostko, N. Heine, M. Ahmed and K. R. Wilson, Probing the Heterogeneous Ozonolysis of Squalene Nanoparticles by Photoemission, *J. Phys. Chem. A*, 2016, **120**, 8645–8656.
- 44 R. Weber, B. Winter, P. M. Schmidt, W. Widdra, I. V. Hertel, M. Dittmar and M. Faubel, Photoemission from aqueous alkali-metal-iodide salt solutions using EUV synchrotron radiation, *J. Phys. Chem. B*, 2004, **108**, 4729–4736.
- 45 J. M. Laux, T. F. Fister, B. J. FinlaysonPitts and J. C. Hemminger, X-ray photoelectron spectroscopy studies of the effects of water vapor on ultrathin nitrate layers on NaCl, *J. Phys. Chem.*, 1996, **100**, 19891–19897.
- 46 D. E. Starr, E. K. Wong, D. R. Worsnop, K. R. Wilson and H. Bluhm, A combined droplet train and ambient pressure photoemission spectrometer for the investigation of liquid/vapor interfaces, *Phys. Chem. Chem. Phys.*, 2008, **10**, 3093–3098.
- 47 S. Ghosal, J. C. Hemminger, H. Bluhm, B. S. Mun, E. L. D. Hebenstreit, G. Ketteler, D. F. Ogletree, F. G. Requejo and M. Salmeron, Electron spectroscopy of aqueous solution interfaces reveals surface enhancement of halides, *Science*, 2005, **307**, 563–566.
- 48 S. Ghosal, A. Shbeeb and J. C. Hemminger, Surface segregation of bromine in bromide doped NaCl: implications for the seasonal variations in Arctic ozone, *Geophys. Res. Lett.*, 2000, **27**, 1879–1882.
- 49 E. R. Mysak, D. E. Starr, K. R. Wilson and H. Bluhm, Note: a combined aerodynamic lens/ambient pressure x-ray photoelectron spectroscopy experiment for the on-stream investigation of aerosol surfaces, *Rev. Sci. Instrum.*, 2010, **81**, 016106.
- 50 A. Lindblad, J. Soderstrom, C. Nicolas, E. Robert and C. Miron, A multi purpose source chamber at the PLEIADES beamline at SOLEIL for spectroscopic studies of isolated species: cold molecules, clusters, and nanoparticles, *Rev. Sci. Instrum.*, 2013, **84**, 113105.
- 51 F. X. Ouf, P. Parent, C. Laffon, I. Marhaba, D. Ferry, B. Marcillaud, E. Antonsson, S. Benkoula, X. J. Liu, C. Nicolas, E. Robert, M. Patanen, F. A. Barreda, O. Sublemontier, A. Coppalle, J. Yon, F. Miserque, T. Mostefaoui, T. Z. Regier, J. B. A. Mitchell and C. Miron, First in-flight synchrotron X-ray absorption and photoemission study of carbon soot nanoparticles, *Sci. Rep.*, 2016, **6**, DOI: [10.1038/srep36495](https://doi.org/10.1038/srep36495).
- 52 A. R. Abid, M. Reinhardt, N. Boudjemia, E. Pelimanni, A. R. Milosavljevic, C. M. Saak, M. Huttula, O. Bjorneholm and M. Patanen, The effect of relative humidity on CaCl₂ nanoparticles studied by soft X-ray absorption spectroscopy, *RSC Adv.*, 2021, **11**, 2103–2111.
- 53 M. I. Jacobs, B. Xu, O. Kostko, A. A. Wiegel, F. A. Houle, M. Ahmed and K. R. Wilson, Using Nanoparticle X-ray Spectroscopy to Probe the Formation of Reactive Chemical Gradients in Diffusion-Limited Aerosols, *J. Phys. Chem. A*, 2019, **123**, 6034–6044.



